Temperature-dependent multilayer relaxation of clean and hydrogen-dosed Nb(100)

D. Lacina and J. L. Erskine
Department of Physics, The University of Texas at Austin, Austin, Texas 78712, USA
(Received 17 May 2007; published 11 September 2007)

Low-energy-electron-diffraction intensity measurements and multiple scattering analysis are used to determine the multilayer surface relaxation of clean and hydrogen-dosed Nb(100) as a function of temperature. Accurate characterization of residual surface impurity concentration (oxygen) based on Auger electron spectroscopy is used to obtain a meaningful extrapolation of the first-layer relaxation to the clean surface value: $d_{12}=1.481\pm.05$ Å corresponding to $\Delta_{12}=-10\pm3\%$, a 10% relaxation relative to the bulk value $d_0=1.645$ Å. This experimental result for d_{12} can be used to judge the accuracy of recent *ab initio* calculations for Nb(100). Temperature-dependent changes in surface relaxation resulting from hydrogen dosing of Nb(100) manifest an expansion of the near-surface lattice resulting from subsurface hydrogen atoms. The hydrogen-induced expansion of near-surface interplanar separation is determined to be $3\pm1\%$ at $T=125$ K, $4\pm1\%$ at $T=300$ K, and $-1\pm1\%$ at $T=400$ K. The measured hydrogen-induced surface lattice expansion is consistent with the bulk lattice constant change ($\Delta\sim4.5\%$) that occurs when Nb is hydrated to form βNbH. The observed relaxation of the hydrogen-dosed near-surface interplanar separation to the clean surface value for $T>400$ K is consistent with the subsurface "hydrogen valve" model that has been used to account for unusual hydrogen uptake kinetics associated with Nb(100).

DOI: 10.1103/PhysRevB.76.104103 PACS number(s): 61.14.Hg, 68.35.Bs, 66.30.Jt, 68.43.Fg

I. INTRODUCTION

The intrinsic properties of Nb and the interaction of hydrogen and oxygen with Nb surfaces are subjects of considerable interest because of the technological importance and physical and chemical properties associated with Nb and its surfaces.[1,2] Nb has the highest superconducting transition temperature of all elemental metals.[3] Nb and other group VB metals exhibit extremely high mobility of hydrogen, and have been widely used as prototype materials for studying metal-hydrogen interactions, including both quantum-mechanical and classical diffusion processes.[2] The surface properties of Nb(100) offer special interest: unlike (bcc) W(100) and Mo(100), which exhibit reversible temperature-dependent reconstruction,[4] Nb(100) maintains a $p(1\times1)$ structure. Hydrogen uptake by Nb(100) has been extensively studied[5–9] because of the hydrogen adsorption and/or desorption behavior manifested by this surface. The chemical effects have been attributed to subsurface hydrogen sites that affect the admission of hydrogen into the bulk and govern surface hydride formation.

While the surface electronic structure of Nb(100) has been investigated by photoemission,[10–13,4,15,16] and the vibrational properties have been investigated by inelastic electron[17] and He atom[18] scattering, the only attempt at a surface structure determination appears to be a study of photoelectron diffraction.[19] There are numerous *ab initio* calculations that explore the electronic, vibrational, and structural properties of bulk Nb,[20] Nb hydrides,[21] and Nb surfaces,[22–25] but there appear to be no prior measurements of closely related multilayer surface relaxation of any Nb surface by low-energy-electron diffraction (LEED).

This paper presents a LEED investigation of multilayer relaxation of Nb(100) including the effects of hydrogen. The results are relevant to recent *ab initio* calculations of surface properties of reactive transition metal surfaces, and various prior studies of hydrogen uptake kinetics and chemisorption of hydrogen at N(100). These prior studies suggest that the properties associated with the hydrogen-Nb(100) surface are governed by hydrogen atoms at tetrahedral lattice sites near the surface. The results also extend our study[26–29] of trends in multilayer relaxation of reactive transition metal surfaces. This experimental program was stimulated by systematic inconsistencies[30,31] between top-layer relaxation obtained from *ab initio* calculations and corresponding results from LEED crystallography.

II. SAMPLE PREPARATION

In situ cleaning, surface characterization, and structure measurements were carried out using an UHV instrument that incorporates LEED, Auger electron spectroscopy (AES), electron-energy-loss spectroscopy, and ultraviolet photoemission capabilities. The LEED intensity-versus-voltage (*I-V*) spectra were measured using frame-grabbing instrumentation interfaced to a SIT camera. The instrument has been used in prior LEED[26–29] and inelastic electron scattering[17] studies, and the LEED methodology has been described in prior publications.[26–29]

Clean surface preparation of Nb(100) presents significant challenges as noted in prior publications.[1,12–14,17,18] The problems are very similar to those encountered for V(100).[29] Nb is a 4*d* metal that lies just below V (3*d* metal) in the Periodic Table. Both V and Nb exhibit high reactivity to and solubility of hydrogen and other elements, including carbon and oxygen. The best efforts to date have yielded only technically clean surfaces of both V(100) and Nb(100). In the case of V(100), bulk carbon limits the cleanliness of a prepared surface to 4%–5% carbon;[29,32] for Nb(100), the strong chemical affinity, high solubility, and high desorption temperature associated with oxygen and the Nb surface have limited the purity of technically clean Nb(100) to about 8%

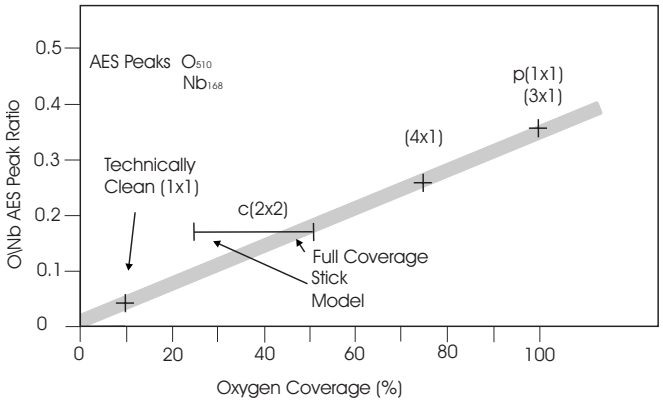

FIG. 1. Nb_{168}/O_{510} Auger electron spectroscopy peak ratios for calibrated oxygen coverages on Nb(100) based on scanning tunneling microscopy experiments of An *et al.* (Ref. 1). The (3×1) Nb(100) reconstruction occurs at saturation oxygen coverage. The point labeled "technically clean" corresponding to an AES peak ratio of 0.4 represents the lower limit of the surface oxygen concentration achieved in the experiments (8%–10%).

oxygen. Fortunately, recent detailed characterization of ordered surface chemisorbed layers [oxygen for Nb(100) (Ref. 1) and carbon for V(100) (Refs. 32 and 33)] based on AES and scanning tunneling microscopy (STM) has established accurate adsorbate coverages referenced to AES peak ratios, and these surface coverage calibrations permit extrapolation of LEED measurements of the multilayer relaxation of technically clean surfaces to clean surface values.[29]

Figure 1 summarizes AES peak ratios (O_{510}/Nb_{168}) for ordered oxygen overlayer models based on STM studies of oxygen-dosed Nb(100).[1] The plotted coverage is based on the fraction of fourfold Nb(100) sites filled by oxygen atoms. The STM images reveal islands and some top-layer Nb atom reconstruction that reduce the effective coverage compared to an ideal coverage model. In the case of the $c(2\times2)$ structure, a "stick" structure reduces the coverage from the ideal value $\left(\Theta=\frac{1}{2}\right)$ to $\Theta=\frac{1}{4}$. This stick reconstruction behavior brings the $c(2\times2)$ oxygen AES peak ratio into reasonable agreement with the coverage-dependent ratios established for the other ordered layers. The lowest O_{510}/Nb_{168} peak ratio achieved in our extensive efforts to clean Nb(100) was $O_{510}/Nb_{168}\gtrapprox0.04$ which according to the calibration data (Fig. 1) corresponds to an oxygen contamination level of about 8%.

Because of the relatively high mobility of oxygen in Nb, it is possible to attribute some uncertainty to the calibration of surface oxygen contamination in terms of the AES O/Nb peak ratio based on STM images, because STM is not sensitive to subsurface oxygen. However, there is no evidence[17] that the oxygen present at a technically clean Nb(100) surface is below the surface (as is clearly the case for hydrogen); therefore, the oxygen AES calibration result obtained from Fig. 1 is believed to be accurate.

Our Nb(100) crystal was prepared and cleaned using the same techniques described for V(100).[29] The crystal was cut from an aligned high-purity (99.99%) boule using a moving-wire electrode and aligned using x-ray Laue methods with the assistance of ORIENT EXPRESS (Ref. 34) software. Initial cleaning and AES analysis of surface impurities revealed carbon, sulfur, and oxygen after several cycles of Ne ion sputtering and annealing. Extensive cycles of ion sputtering and annealing to within 200 K of the melting temperature (2740 K) yielded a technically clean Nb(100) surface that was free of all impurities (except oxygen) to the sensitivity limit of AES (estimated to be 1%), and an oxygen concentration of about 8%.

III. LOW-ENERGY-ELECTRON-DIFFRACTION DATA AND ANALYSIS

LEED intensity-versus-voltage (*I-V*) data sets were acquired after symmetrizing conjugate (symmetry-degenerate) beam intensities as described previously.[26–29] Typical Pendry (r_P) and Zanazzi-Jona (r_{ZJ}) r factors for conjugate beam and/or averaged beam comparison of unsmoothed *I-V* spectra for five "clean" Nb(100) data sets are as follows: (10) beams (450 eV range) $r_P\sim0.163$, $r_{ZJ}\sim0.052$; (11) beams (350 eV range) $r_P\sim0.152$, $r_{ZJ}\sim0.052$; (20) beams (300 eV range) $r_P\sim0.124$, $r_{ZJ}=0.055$; (21) beams (200 eV range) $r_P\sim0.156$, $r_{ZJ}\sim0.041$. Corresponding values for five hydrogen-dosed Nb(100) data sets are as follows: (01) beams, $r_P\sim0.136$, $r_{ZJ}\sim0.028$; (11) beams, $r_P\sim0.159$, $r_{ZJ}\sim0.048$; (20) beams, $r_P\sim0.146$, $r_{ZJ}\sim0.047$; (21) beams, $r_P\sim0.145$, $r_{ZJ}\sim0.040$. The low r factors indicate good alignment of the incident beam along the (100) crystal axis.

The Barbieri/Van Hove SATLEED code[35] was used to numerically simulate the measured *I-V* spectra. A typical example of an optimized simulation is shown in Fig. 2 with the corresponding *I-V* data set and r factors that characterize the fit. The calculations are based on 13 relativistic phase shifts, which were also calculated using the Barbieri/Van Hove code. Convergence tests in which r factors and structure parameters were evaluated as a function of the number of phase shifts used in the analysis revealed no differences for $l_{max}\geqslant6$. Standard r factor analysis based on r_P and r_{ZJ} was used to optimize structural and nonstructural parameters leading to structure determination based on the *I-V* spectra. The application of both r_P and r_{ZJ} criteria yielded essentially the same structural results. All calculations for both technically clean and hydrogen-dosed Nb(100) were carried out using a surface structural model that allowed multilayer relaxation of the top three layers, but no lateral displacements of the atoms within a plane. This assumption is consistent with STM studies[1] of Nb(100) and with the $p(1\times1)$ LEED patterns observed in our experiments that manifest no evidence of surface reconstruction.

LEED simulations for the hydrogen-dosed Nb(100) surface were carried out using the same multiple scattering model (crystal unit cell) used for the clean surfaces. Neglecting the weak scattering from hydrogen atoms is justified, based on our prior LEED experiments on clean and hydrogen-dosed Rh(001).[26] In that study, two structural models were applied to experimental *I-V* spectra obtained from a saturated coverage of H on Rh(100). One model neglected scattering from hydrogen atoms, and the second model included hydrogen atoms in the (lowest total energy) fourfold

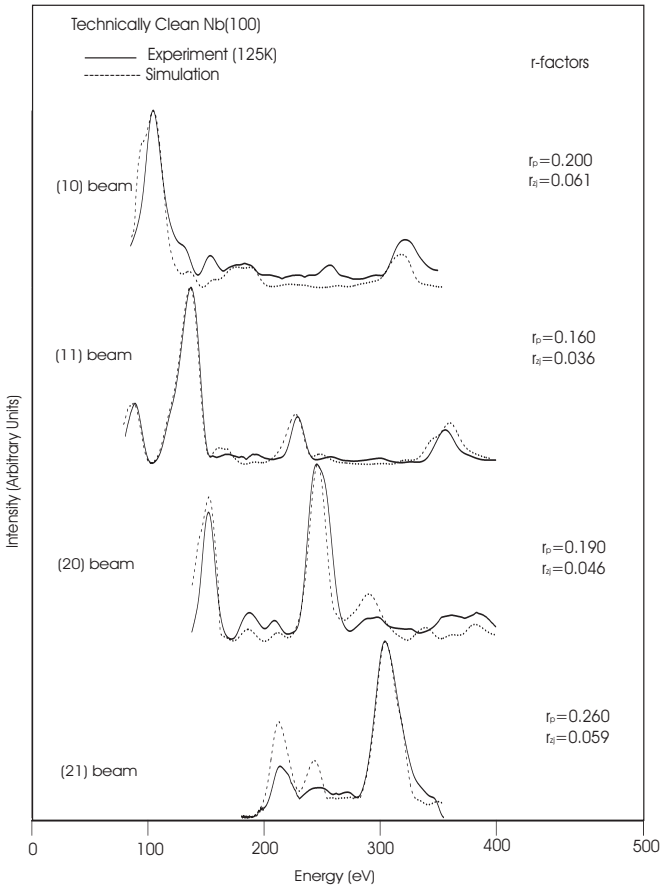

FIG. 2. LEED intensity spectra for Nb(100) plotted with corresponding intensity simulations and Pendry (r_P) and Zanazzi-Jona (r_{ZJ}) r factors that characterize the fit.

hollow sites. Both simulations converged to the same model for the multilayer surface relaxation (within ±0.01 Å). Based on multilayer relaxation results for hydrogen-dosed Nb(100), presented later, a LEED I-V analysis was also carried out assuming that the bulk Nb(100) surface was terminated by a single unit cell of bulk βNbH. This model did not provide a better fit to experimental data for hydrogen-dosed Nb(100).

IV. TECHNICALLY CLEAN AND CLEAN Nb(100) STRUCTURE

Density-functional-theory calculations provide a means of studying trends in physical parameters associated with metal surfaces such as surface energies, work functions, and surface relaxation, as well as chemical phenomena such as chemisorption.[23,36] The study of trends for high-index crystallographic surfaces of a series of metals (for example, the 4d transition metals) offers important opportunities for testing simple models of surface behavior and for gaining insight into the physical processes that govern the trends. For example, the tendency of sp electrons to spread smoothly at a surface, coupled with the directional forces associated with localized d electrons, has been used to account for various trends observed in the surface relaxations and chemical behavior of transition metal surfaces.

A key element in assessing the validity and accuracy of *ab initio* calculations of surface properties has been the comparison of calculated multilayer surface relaxation with corresponding results obtained by electron-diffraction experiments. Tests based on other information, such as work functions, occurrence of magnetic ordering or magnetic dead layers, the tendency of certain bcc surfaces [i.e., W(100) and Mo(100)] to reconstruct, and electronic structure specific to a surface (electronic surface states and resonances), have also been used to test predictive accuracy of *ab initio* calculations, but multilayer surface relaxation seems to have become the traditional standard test. This is a logical choice because the position and coordination of surface atoms is a ground state property that governs other physical properties, including surface and thin-film magnetism and surface electronic structure; the structure can, in principle, be accurately determined (by LEED). The use of electronic binding energies and bandwidths determined by photoemission as a means of evaluating accuracy of calculations may be a less favorable criteria because these parameters involve excitations that introduce questions about energy shifts resulting from many-body effects.

Although the comparison of calculated and measured multilayer surface relaxations has been adopted as one of the most important tests of the predictive accuracy of *ab initio* methodology, significant (and apparently systematic) discrepancies between experimentally and theoretically determined multilayer relaxations have been noted.[30,31] *Ab initio* methods generally reproduce quite accurately bulk lattice parameters obtained by x-ray diffraction; therefore, the corresponding discrepancies for surface structure, which in many cases exceeds the claimed accuracy of both the LEED methodology and the calculations, has caused some concern. Some of the existing discrepancies have been recently accounted for in terms of the effects driven by low concentrations of (undetected) hydrogen[28] or other surface impurities[29,32] that increase the coordination of surface atoms. Increased coordination of surface atoms tends to reduce top-layer relaxations. These results justify reevaluation of some of the existing LEED structure determinations with special attention to the level of surface impurities, as well as new LEED experiments using surfaces for which *ab initio* calculations have included predictions of multilayer relaxation, i.e., Nb(100).

Table I summarizes the available surface structure information for Nb(100) derived from *ab initio* calculations, and from the only existing experimental result (based on photoelectron diffraction) for top-layer relaxation. The results displayed in Table I represent one of the few cases where an existing experimentally determined top-layer relaxation is greater than typical values obtained from *ab initio* calculations. Also summarized in Table I are our LEED results for Δ_{ij} for extrapolated clean, technically clean (~8% oxygen). Hydrogen-dosed experiments are described in the following section.

Figure 3 displays values of Δ_{12} and Δ_{23} for Nb(100) with an ordered $c(2\times2)$ oxygen surface layer and for technically clean $p(1\times1)$ Nb(100) with an estimated (disordered) oxygen concentration of ~8%. The oxygen concentration is based on the AES calibration described in Fig. 1. The r_P

TABLE I. Calculated and measured surface relaxations for Nb(100). Interplanar relaxations $\Delta_{ij}=d_{ij}/d_o$ are presented as a percentage of the bulk lattice separation d_o.

Calculation	Δ_{12}	Δ_{23}	Δ_{34}
TBA 20 layer slab[a]	−11.65		
TBA[b]	−12.1	+10.7	−5.6
DFT/LDA 7 layer slab[c]	−9.3		
TBA/MD[d]	−6.3	−0.7	
Experiment			
Photoelectron diffraction[e]	−13.5		
LEED (extrapolated)	−10.0	+5.5	
LEED [(1×1) 9% oxygen]	−7.2	+3.5	−3.1
[(2×2) 20% oxygen]	−5.2	+1.7	+3.6

[a]Reference 25.
[b]Reference 24.
[c]Reference 23.
[d]Reference 22.
[e]Reference 19.

values obtained in fits for $p(1\times1)$ technically clean Nb and $c(2\times2)$ oxygen on Nb(100) are low enough to be able to place high confidence in the LEED-determined value of Δ_{ij}. For example, similar values of r_P were obtained in our prior LEED analysis of clean Rh(100), $r_P\sim0.30$ for 100 K data sets; W(100), $r_P\sim0.202$ for 400 K data sets; technically clean Ti(0001), $r_P\sim0.140$ for 125 K data sets, and technically clean V(100), $r_P\sim0.223$ for 150 K data sets. In these prior experiments, technically clean surfaces corresponded to 20% hydrogen for Ti(0001) and 6% carbon for V(100). Our extrapolated clean surface value of Δ_{12} is in good agreement with the result obtained from the most recent *ab initio* calculation.

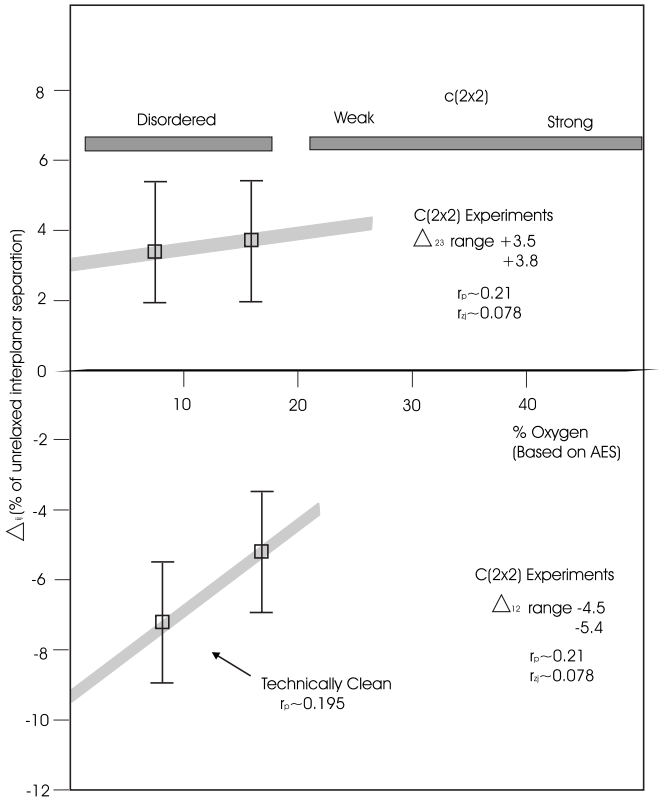

FIG. 3. Graphical illustration of the range of ordered $c(2\times2)$ and disordered chemisorbed oxygen on Nb(100) with LEED values for first (Δ_{12}) and second (Δ_{23}) layer relaxations at two oxygen concentrations. The extrapolated value of Δ_{12} to zero oxygen coverage is $\Delta_{12}\sim-10\%$.

V. HYDROGEN-DOSED Nb(100)

Table II presents a more detailed account of experimental results for Δ_{ij} obtained from LEED analysis of technically clean and hydrogen-dosed Nb(100). Several data sets were obtained at three temperatures. The minor differences in Δ_{ij} at different temperatures are attributed to the ability of Nb to absorb hydrogen into the bulk, especially at elevated temperature, and the fact that the best technically clean Nb(100) surfaces exhibited easily detected (by AES) oxygen contamination (~8%). The hydrogen contamination of the technically clean Nb(100) was judged low (<1%) based on the base pressure ($\sim5\times10^{-11}$ torr) and previous experience with evaluating the effects of hydrogen contamination at similar base pressure.[28,29]

The hydrogen-dosed surface structural data exhibit temperature-dependent trends in multilayer relaxation that are consistent with prior photoemission,[10–16] inelastic electron scattering,[17] and adsorption and/or desorption kinetics[5–8] experiments that probe the hydrogen-Nb(100) surface system. These experiments probed temperature-dependent electronic (photoemission) and vibrational (inelastic electron scattering) properties associated with hydrogen-dosed Nb(100) that were interpreted to result from the effects of hydrogen in tetrahedral subsurface sites. Both experiments exhibited reversible temperature-dependent effects produced by hydrogen dosing that provided indirect experimental evidence of the self-trapped subsurface state model which has been proposed to account for the kinetics of hydrogen uptake by Nb.[5–10] Our LEED results for multilayer surface relaxation of hydrogen-dosed Nb(100) provide more direct evidence for the subsurface hydrogen sites and additional support for the model of uptake kinetics based on these sites.

Figure 4 displays a side-view model of the (bcc) Nb(100) surface with symbols that describe various lattice plane displacements and separations. Table III defines the parameter Δ_i and lists (normalized) values of Δ_1 and Δ_2 obtained from temperature-dependent multilayer relaxation of clean and hydrogen-treated Nb(100). Entries of Table III that are noted by * highlight values of Δ_2 that manifest significant changes resulting from hydrogen dosing or changes in temperature. The significant changes in Δ_2 resulting from hydrogen dosing result primarily from the large changes of Δ_{34} (Table II) that occur after hydrogen dosing of Nb(100) below 400 K. Note that Δ_2 characterizes the separation of crystallographic planes just below the surface. The change in Δ_2 resulting from hydrogen dosing below 400 K corresponds to a unit-cell distortion along the (100) direction of 3%–4%. Formation of bulk NbH results in a change in the (bcc) lattice

TABLE II. Multilayer relaxation determined by LEED for technically clean Nb(100) and (1L) hydrogen-dosed Nb(100) at three temperatures. Pendry (r_P) and Zanazzi-Jona (r_{ZJ}) r factors associated with experiment and/or simulation are displayed for each structure determination.

	T(K)	Δ_{12}	Δ_{23}	Δ_{34}	r_P	r_{ZJ}
Clean	125	−7.2	+3.5	−3.1	0.196	0.049
	125	−7.7	+3.6	−3.3	0.160	0.035
	300	−6.9	+3.6	−4.2	0.213	0.039
	300	−6.4	+3.3	−4.0	0.217	0.046
	400	−6.5	−1.4	−5.7	0.188	0.052
Hydrogen	125	−4.5	+5.7	−5.4	0.201	0.074
	125	−4.7	+5.7	−3.6	0.199	0.065
	300	−5.0	+4.5	−8.0	0.250	0.083
	300	−5.5	+2.7	−8.0	0.195	0.055
	400	−6.0	+3.6	−3.0	0.163	0.069

constant from a_o=3.29 Å to a_o=3.44 Å (β phase) or a_o =3.46 (δ phase) corresponding to an expansion of 4.5% (β phase) or 5.2% (δ phase).

The observed changes in multilayer surface relaxation of technically clean Nb(100) as a function of temperature for a hydrogen-dosed surface are consistent with prior experiments that explore subsurface hydrogen at Nb(100). The results manifest strong evidence of lattice expansion for T $<$400 K attributed to hydrogen atoms occupying tetrahedral sites in the lattice near the surface. The measured expansion of the near-surface lattice (Δ_2=separation between second and third lattice planes) is 3±1% at 125 K, 4±1% at 300 K, and −1±1% at 400 K. The expansion at T<400 K is compatible with the change in lattice constant when Nb is hydrated to βNbH (4.5% increase). The relaxation of the lattice expansion to the clean surface value for T>400 K is consistent with thermally driven depopulation of the near-surface hydrogen sites that has been used to explain temperature-dependent changes in the surface electronic and vibrational properties of hydrogen-dosed Nb(100) which supports the subsurface-valve model of hydrogen uptake kinetics associated with Nb(100).

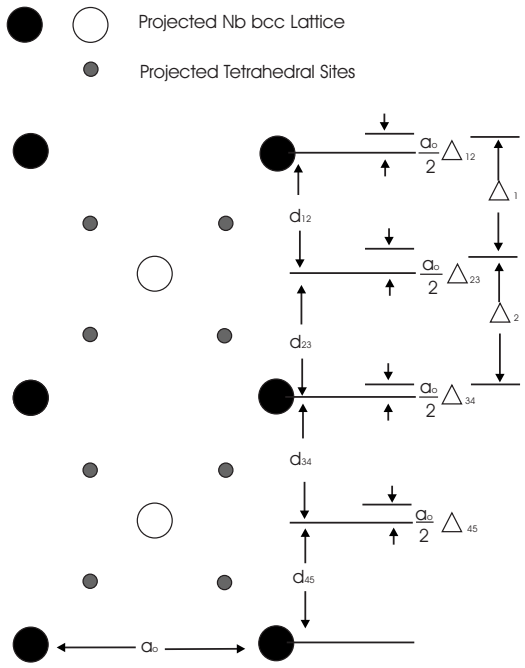

FIG. 4. Side view of Nb(100) lattice showing projected location of hydrogen (tetrahedral sites) and defining the parameters a_o lattice constant, d_{ij} interplanar separation, Δ_{ij} relaxation parameter, and Δ_i interplanar expansion parameter.

VI. SUMMARY

The surface structure of Nb(100) has been investigated by LEED crystallography as a function of temperature and as a function of oxygen coverage and hydrogen dose. The multilayer relaxation of $c(2\times2)$ O on Nb(100) and technically clean $p(1\times1)$ surfaces with ~8% oxygen contamination were determined by LEED and used to extrapolate the value of top-layer relaxation to a clean surface value d_{12} =1.481±0.05 Å corresponding to a contraction of −10.0±3%. The value is in reasonably good agreement with recent *ab initio* calculations that predict a first-layer contraction at Nb(100) of 10%–12% (Table I). The only other available experimental result for d_{12} at Nb(100) is based on photoelectron diffraction d_{12}=13±5% (Table I). Thus, the two experiments are compatible based on the error estimates. The photoelectron-diffraction result is not accompanied by a meaningful quantitative assessment of the surface oxygen or hydrogen concentration; therefore, any additional comparison or discussion of the two experimental values is unjustified.

Surface vibrational modes for hydrogen-dosed Nb(100) (Ref. 17) are consistent with hydrogen atoms at subsurface tetrahedral sites of the Nb lattice (β phase of NbH). Both vibrational spectroscopy[17] and photoemission spectroscopy[14] experiments indicate the existence of a reversible phase transition associated with subsurface site occupancy by hydrogen at Nb(100) that occurs in the temperature range 300$\leqslant T$ $\leqslant$600 K. The hydrogen-induced variation of Δ_2 determined by LEED and displayed in Table III is consistent with the

TABLE III. Temperature-dependent near-surface lattice expansion ($2\Delta/a_o > 1$) or contraction ($2\Delta/a_o < 1$) relative to bulk Nb value $a_o/2$ for clean and hydrogen-dosed Nb(100). Note that normalized values of Δ_I ($2\Delta_i/a_o$) are shown in the table. Table entries highlighted by * exhibit significant temperature-dependent and hydrogen-dose dependent changes.

			125 K	300 K	400 K
$\Delta_1 \equiv \frac{a_o}{2}(1+\Delta_{12}-\Delta_{23})$	$\frac{2\Delta_1}{a_o}$	Clean	0.89	0.89	0.90
		Hydrogen	0.90	0.91	0.90
$\Delta_2 \equiv \frac{a_o}{2}(1+\Delta_{23}-\Delta_{34})$	$\frac{2\Delta_2}{a_o}$	Clean	1.07	1.08	1.07
		Hydrogen	1.10*	1.12*	1.06
Bulk Nb	$a_o=3.29$				
δNbH	$a_o=3.46$ (5.2% expansion)				
βNbH	$a_o=3.44$ (4.5% expansion)				

previously observed reversible phase transition involving subsurface hydrogen sites at Nb(100), and provides direct structural evidence for the surface-valve model based on measured expansion of the near-surface lattice.

ACKNOWLEDGMENT

The work was supported by the Robert A. Welch foundation, Grant No. F-1015.

[1] B. An, S. Fukuyama, K. Yokogawa, and M. Yoshimura, Phys. Rev. B **68**, 115423 (2003).
[2] N. Shamir, U. Atzmony, J. A. Schultz, and M. H. Mints, J. Vac. Sci. Technol. A **5**, 1024 (1987).
[3] H. R. Schober and A. M. Stoneham, Phys. Rev. Lett. **60**, 2307 (1988).
[4] T. E. Felter, R. A. Barker, and P. J. Estrup, Phys. Rev. Lett. **38**, 1138 (1977).
[5] M. Lagos, J. Rogan, and I. K. Schuller, Phys. Rev. B **44**, 3380 (1991).
[6] S.-W. Kim and K.-S. Sohn, Phys. Rev. B **40**, 1003 (1989).
[7] M. Lagos, G. Martinez, and I. K. Schuller, Phys. Rev. B **29**, 5979 (1984).
[8] M. Lagos and I. K. Schuller, Phys. Rev. B **32**, 5477 (1985).
[9] G. J. Dienes, M. Strongin, and D. O. Welch, Phys. Rev. B **32**, 5475 (1985).
[10] R. J. Smith, Phys. Rev. Lett. **45**, 1277 (1980).
[11] W. Eberhardt, F. Greuter, and E. W. Plummer, Phys. Rev. Lett. **46**, 1085 (1981).
[12] B.-S. Fang, C. A. Ballentine, and J. L. Erskine, Phys. Rev. B **38**, 4299 (1988).
[13] B.-S. Fang, C. A. Ballentine, and J. L. Erskine, Phys. Rev. B **36**, 7360 (1987).
[14] B.-S. Fang, C. A. Ballentine, and J. L. Erskine, Surf. Sci. **204**, L713 (1988).
[15] B.-S. Fang, W.-S. Lo, and H. H. Chen, Phys. Rev. B **47**, 10671 (1993).
[16] B.-S. Fang, W.-S. Lo, T.-S. Chien, T. C. Leung, C. Y. Lue, C. T. Chan, and K. M. Ho, Phys. Rev. B **50**, 11093 (1994).
[17] Y. Li, J. L. Erskine, and A. C. Diebold, Phys. Rev. B **34**, 5951 (1986).
[18] E. Hulpke, M. Hüppauff, D.-M. Smilgies, A. D. Kulkarni, and F. W. deWette, Phys. Rev. B **45**, 1820 (1992).
[19] W.-S. Lo, T.-S. Chien, B.-S. Fang, C. M. Wei, and W. N. Mei, Surf. Rev. Lett. **5**, 1035 (1998).
[20] A. R. Jani, N. E. Brener, and J. Callaway, Phys. Rev. B **38**, 9425 (1988).
[21] K.-M. Ho, H.-J Tao, and X.-Y. Zhu, Phys. Rev. Lett. **53**, 1586 (1986).
[22] J. S. Luo and B. Legrand, Phys. Rev. B **38**, 1728 (1988).
[23] M. Methfessel, D. Hennig, and M. Scheffler, Phys. Rev. B **46**, 4816 (1992).
[24] M. Brejnak and P. Modrak, Surf. Sci. **310**, L614 (1999).
[25] Ch. E. Lekka, M. J. Mehl, N. Bernstein, and D. A. Papaconstantopoulos, Phys. Rev. B **68**, 035422 (2003).
[26] G. Teeter, D. Hinson, J. L. Erskine, C. B. Duke, and A. Paton, Phys. Rev. B **57**, 4073 (1998).
[27] G. Teeter, J. L. Erskine, F. Shi, and M. A. Van Hove, Phys. Rev. B **60**, 1975 (1999).
[28] G. Teeter and J. L. Erskine, Phys. Rev. B **61**, 13929 (2000).
[29] D. Lacina, J. Yang, and J. L. Erskine, Phys. Rev. B **75**, 195423 (2007).
[30] P. J. Feibelman, Surf. Sci. **360**, 297 (1996).
[31] P. J. Feibelman, Phys. Rev. B **53**, 13740 (1996).
[32] W. Bergermayer, R. Koller, C. Konvicka, M. Schmid, G. Kresse, J. Redinger, P. Varga, and P. Podloucky, Surf. Sci. **497**, 294 (2002).
[33] M. Beutl, J. Lesnik, E. Lundgren, C. Konvicka, P. Varga, and K. D. Rendulic, Surf. Sci. **447**, 245 (2000).
[34] Jean Laugier and Bernard Bochu, ORIENT EXPRESS, ENSP/ Laboratoire des Materiaux et du Genie Physique, BP46, Saint Martin d'Heres, France, http://www.inpg.fr/LMGP and http://www.ccp14.ac.uk/tutorial/lmg
[35] A. Barbieri and M. A. VanHove, automated tensor LEED program, available from M. A. VanHove at Lawrence Berkeley Laboratory.
[36] M. Scheffler and C. Stampfl, *Handbook of Surface Science*, edited by K. Horn and M. Scheffler (Elsevier, Amsterdam, 1999), Vol. 2.